Energy Conversion and Management: X 13 (2022) 100147

Contents lists available at ScienceDirect

Energy Conversion and Management: X

journal homepage: www.sciencedirect.com/journal/energy-conversion-and-management-x

Thermo-kinetic study to explicate the bioenergy potential of Holy Thistle (HT)

Hesham Alhumade [a,b], Jean Constantino Gomes da Silva [c], Emanuele Mauri [d], Muhammad Sajjad Ahmad [e], Yusuf Al-Turki [f], Nagaraju Pasupulety [a], Ali Elkamel [e,*]

[a] Department of Chemical and Materials Engineering, Faculty of Engineering, King Abdulaziz University, Jeddah 21589, Saudi Arabia
[b] Center of Excellence in Desalination Technology, King Abdulaziz University, Jeddah, Saudi Arabia
[c] Department of Chemical Engineering and Food Engineering, Federal University of Santa Catarina, 88040-900 Florianópolis Santa Catarina, Brazil
[d] Department of Engineering, Università Campus Bio-Medico di Roma, via Álvaro del Portillo 21, 00128 Rome, Italy
[e] Department of Chemical Engineering, University of Waterloo, Waterloo, Canada
[f] Department of Electrical and Computer Engineering, Faculty of Engineering, King Abdulaziz University, Jeddah 21589, Saudi Arabia

ARTICLE INFO

Keywords:
Waste biomass
Pyrolysis
Thermodynamics parameters
Bioenergy
Pyrolysis products

ABSTRACT

Biomass is one of the key components for bioenergy generation in recent epoch as traditional resources and depleting swiftly. Going through this fact, the present study aims to appraise the feasibility of Holy Thistle (HT) to produce energy and valuable organic chemicals through pyrolysis. The HT was pyrolyzed at four heating rates including, 10, 20, 30, and 40 °C min^{-1} to perform thermo kinetic modeling and estimate thermodynamics parameters to establish the pyrolysis reaction process. The pyrolysis process of HT illustrated about 85–88 % of thermal degradation achieved through three different stages from 30 to 800 °C. The major degradation stage was observed from 170 to 450 °C with 55% to 60 % product formation from mainly cellulose and hemicelluloses components. Moreover, the average activation energy and pre-exponential factors demonstrated to be 183–184 kJ mol^{-1} and 10^{10} min^{-1} to 10^{25} min^{-1}, respectively. The pyrolytic products exhibited agreement to the cleaner production of bio-gas, char and bio-oil which is evident for the potential and productivity of the feed combination.

Introduction

As fossil fuels fulfill the energy requirements of world in current times, fossil fuels are likely to be consumed in about 70 years [1], thus paving a way for some alternative fuel source i.e. biomass, solar, wind and hydrothermal. In comparison, biomass is likely to be reliable energy source, since this feedstock has a low market value than fossil fuel, found abundantly in nature, and its use generates low greenhouse gas emissions. Biomass contributes almost 10% of all the other available energy sources worldwide, and its usage is annually increasing at the rate of 2.5% [2]. In some countries like USA and Brazil, 80% of their energy requirements are fulfilled by bio-renewable sources i.e. maize and sugarcane. These energy sources are expensive as well as problematic, causing food versus fuel dilemma. On the other hand, the other available option is to utilize non-arable land to produce edible plants, which would have no direct or indirect competition for food and land, thus, providing cheap alternative to the already available energy resource [3]. However, unavailability of the biomass is not a problem; the challenge is to efficiently extract the stored energy of the biomass through cost-effective methods. There are multiple ways to be used for extraction of energy from biomass: direct combustion, thermochemical and biological conversion. Furthermore, biological fermentation and pyrolysis are old and interesting methods for the reliable conversion of the biomass into a product, but they are cumbersome, expensive and time-taking processes, due to obstinate nature of biomass [4]. As pyrolysis process is a thermal transformation of biomass, under an inert environment (presence of nitrogen) to produce different products like solid, liquid and gases. The pyrolysis process delivers negligible amount of waste as well as all the converted components are pursued for multiple purposes like industrial chemicals (gases), energy (heat, bio-oil) and agricultural (char). However, physicochemical characteristics of biomass, temperature, residence time and particle size are the factors of prime importance for pyrolysis reactor operation. The kinetic study and thermal behavior are important parameters to know about the pyrolysis

* Corresponding author.
E-mail address: aelkamel@uwaterloo.ca (A. Elkamel).

https://doi.org/10.1016/j.ecmx.2021.100147
Received 10 September 2021; Received in revised form 21 November 2021; Accepted 23 November 2021
Available online 30 November 2021

of biomass to make optimized pyrolytic process for conversion of any biomass to valuable products.

While thermogravimetric analysis conducted in controlled conditions is a suitable processes for understanding the pyrolytic behavior and checking for the optimal pyrolytic conditions of any biomass [5–8]. Nevertheless, it is imperative to understand the pyrolytic behavior of any biomass before nourishing the biomass to any commercial thermal plant. The determination of kinetic analysis directly or indirectly influences the economical feasibility of the pyrolysis process, as low activation energy described the weaker bonding between the molecules that demonstrated the lower energy required to achieve desired products and vice versa. It also influences the temperature and reactions conditions to achieve desired chemical and products at specific heating rate that also relate to the economic feasibility of the process.

Several grasses like Sorghum weeds, Miscanthus, Wheat straw, Corn cobs, *typha latifolia*, along with coffee-husk, poplar plotwood pellets, agriculture biomass and *Chrysophyllum albidum* stem bark [9–16], were previously analyzed by using TGA for understanding their bioenergy potential, while Napier grass has been used for fuel production on commercial thermal plants [17]. Inspired by the promising potential of various plant biomass in bioenergy production field, the current study focuses on exploring the bioenergy potential of HT. The current biomass sample was selected based on different factors including the invasive property of the biomass and the possibility of growing the biomass in various environmental conditions.

HT grows in marginal lands and may spread in various environmental conditions such as brackish soil or polluted water to claim as cheapest source for bioenergy production. Biomass growth in such condition may deliver bioremediatory action that can end pollutants causing bitter taste. Therefore, biomasses such as HT are unfit for food or feed. In comparison to fossil fuel, HT may generate 25 units more energy, which can be attributed to its higher energy potential [18]. Since reaction order model substantiates its capability in the entire pyrolysis process, therefore it is considered as a reliable reaction mechanism of the biomasses. The current study also contains high precision thermogravimetric and kinetic analyses of devolatization process [19]In present study, pyrolysis behavior of HT has been studied for the very first time using TGA in order to understand its bioenergy potential, reaction chemistry and pyrolytic behavior. HT is widely grown in all around the world. The major degradation stages with different temperature ranges were determined under different heating rates. Furthermore, kinetic study established a good connection to reveal the bioenergy potential of HT through pyrolysis. It is also a future scope to further study on HT to determine the chemical composition of evolved gases and chemicals through different experimental techniques.

Materials and methods

Elemental composition and proximate analyses

Collection of the biomass of HT was done by collecting from the salinity-hit soil which was under the constant irrigation of the underground brackish water. Distilled water was used to clean the attached impurities from the collected sample and later it was air dried for several days. A manual crusher was used to crush the air-dried biomass of HT and this crushed biomass was placed in oven for 48 h to remove moisture from HT at 105 °C. Particles of varying size ranging from 150 μm to 200 μm was obtained by grinding the sample. This biomass was put through to proximate analyses to evaluate moisture content (%), ash (%) and volatile matter (VM %) with the help of standard protocols as outlined in ASTM (E872-&82 2006, E871-82 2006, E1755-01 2007). Determination of fixed carbon (FC %) was accomplished through the equation: FC (%) = 100-(ash content + VM + moisture). VM and moisture content was calculated by putting the known mass into oven at 380 K (in triplicate) for 16–24 h so that a constant mass could be achieved. By doing so, moisture content was further decreased and so was the biomass of the sample. After this, oven dried sample, having known mass, was placed in a pre-weighed ceramic utensil in triplicate and was put into a Muffle furnace for 3–4 h to have a constant mass of the sample. Loss in mass and ash content of the sample reflected Volatile matter (VM) and residual mass, respectively. An elemental analyzer (Vario EL Cube, Germany) was used to estimate the composition of organic elements like Oxygen (O), Nitrogen (N), Sulphur (S), Hydrogen (H) and Carbon (C). In this analysis, Argon (Ar) was the carrier gas.

The amount of energy that is generated from a biomass is represented by the High Heating Value (HHV). However, expensive experimental procedures and unwanted experimental faults are an obstacle to determine the HHV (MJ kg^{-1}). Therefore, to overcome this problem, several correlation models have been developed to evaluate HHV. In this study, the best suitable correlation model, developed until now, was used to determine HHV [20].

TGA-DSC experiment

STA-409 was used for TGA-DSC analyses, NETZSCH-Gerätebau GmbH, Germany. Calibration was done according to the instruction manual. Later, alumina crucibles were used in a vertical thermobalance for constant heating at 800 °C of 10 mg of milled biomass having particle size between 150 μm and 200 μm. Rate of constant heating was 10, 20, 30 and 40 °C min^{-1}. All experiments were conducted in triplicate to confirm the reproducibility of data. Nitrogen gas flow at the rate of 100 mL min^{-1} was used to maintain an inert environment in the reaction chamber The experimental parameters for TGA in this study were performed based on the International Confederation for Thermal Analysis and Calorimetry (ICTAC) recommendations [21].

Mathematical model development for thermogravimetric analyses

Data of TGA-DSC experiments was analyzed, and a mathematical model was developed. Disintegration rate of the solid sample in isoconversional method is described by Eq. (1), which uses a simplifying assumption about the transformation rate during a reaction is the product of two functions, temperature, T, fraction transformed (conversion), α [1].

$$\frac{d\alpha}{dt} = k(T)\cdot f(\alpha) \tag{1}$$

where k (T) is the reaction rate constant, T is the temperature (K), t is the time (min^{-1}) and α is the conversion represented Eq. (2). This equation indicates that the heterogeneous decomposition kinetics is related to the increase of the temperature and their conversion, or released mass, due to the breakdown of the biomass molecule to generate new compounds.

$$\alpha = \frac{m_0 - m_t}{m_0 - m_\infty} \tag{2}$$

Here α is the conversion, m_0 is the initial mass (mg), m_t is change in the mass (mg), and m_∞ is the residual mass (mg) and

Using k (T), Eq. (1) was re-written as follows;

$$\frac{d\alpha}{dt} = A\cdot exp\left(\frac{-E_\alpha}{R\cdot T}\right)\cdot f(\alpha) \tag{3}$$

Where

A stands for pre-exponential factor (min^{-1})

E stands for activation energy (J mol^{-1})

f(α) is the reaction model

R stands for Universal gas constant (8.314 J K^{-1} mol^{-1})

The conversion rate in Eq. (3) is governed by inherent parameters of the biomass when a temperature change is applied, where the dependence is associated to the activated energy, frequency factor and, reaction model, where these parameters are called of kinetic triplet. The thermal analysis is often performed by the temperature change; thus, the reaction rate is used (β = dT/dt) and results in Eq. (4).

Table 1
List of reaction models often used in solid-state reaction kinetics.

Model	Mechanism	g(α)	f(α)
Nucleation Models			
P2	Power law	$\alpha^{1/2}$	$2\alpha^{1/2}$
P3	Power law	$\alpha^{1/3}$	$3\alpha^{2/3}$
P4	Power law	$\alpha^{1/4}$	$4\alpha^{3/4}$
P2/3	Power law	$\alpha^{3/2}$	$2/3\alpha^{-1/2}$
A2	Avrami-Erofeev	$[-ln(1-\alpha)]^{1/2}$	$2(1-\alpha)[-ln(1-\alpha)]^{1/2}$
A3	Avrami-Erofeev	$[-ln(1-\alpha)]^{1/3}$	$3(1-\alpha)[-ln(1-\alpha)]^{2/3}$
A4	Avrami-Erofeev	$[-ln(1-\alpha)]^{1/4}$	$4(1-\alpha)[-ln(1-\alpha)]^{3/4}$
Reaction Order Models			
F1	First Order Reaction	$-ln(1-\alpha)$	$1-\alpha$
F2	Second Order Reaction	$(1-\alpha)^{-1}-1$	$(1-\alpha)^2$
F3	Third Order Reaction	$(1/2)\left[(1-\alpha)^{-2}-1\right]$	$(1-\alpha)^3$
Fn	n-Order Reaction	$\left[1-(1-a)^{1-n}\right]/(1-n)$	$(1-\alpha)^n$
Geometrical Contraction Models			
R2	Contracting cylinder	$1-(1-\alpha)^{1/2}$	$2(1-\alpha)^{1/2}$
R3	Contracting sphere	$1-(1-\alpha)^{1/3}$	$3(1-\alpha)^{2/3}$
Diffusion Models			
D1	One-dimensional diffusion	α^2	$1/2\alpha^{-1}$
D2	Two-dimensional diffusion	$(1-\alpha)ln(1-\alpha)+\alpha$	$[-ln(1-\alpha)]^{-1}$
D3	Three-dimensional diffusion	$\left[1-(1-\alpha)^{1/3}\right]^2$	$3/2(1-\alpha)^{2/3}\left[1-(1-\alpha)^{1/3}\right]^{-1}$
D4	Ginstling-Brounshtein	$1-(2/3)\alpha-(1-\alpha)^{2/3}$	$3\left[2\left((1-\alpha)^{-1/3}-1\right)\right]^{-1}$

$$\frac{d\alpha}{dT}=\frac{A}{\beta}\cdot exp\left(\frac{-E_\alpha}{R\cdot T}\right)\cdot f(\alpha) \tag{4}$$

Kinetic modeling

Thermal degradation properties of the sample are understood by the kinetic parameters of the pyrolysis reaction. According to International Confederation for Thermal Analysis and Calorimetry (ICTAC), the differential methods should not be considered as being necessarily more accurate and precise than the integral methods, since the differential isoconversional methods is unavoidably associated with certain inaccuracy as well as with imprecision (significant inaccuracy in the rate values, the reaction heat shows a noticeable dependence on heating rate, noisy data) [2]. In this work, these parameters were calculated with the help of isoconversional models as they were designed by FWO (Flynn-Wall-Ozawa), Starink and KAS (Kissenger-Akahira-Sunose) [22–24]. Those methods are also called as p(y)-isoconversional methods since uses approximation equations to solve the integral form of Eq. (4). Several approximations have been suggested in the literature to solve the integral form of Eq. (4), however, FWO, KAS and Starink are the best known, the most cited and the most accurate methods. Starink showed the accurate of each approximation and related to each other. The pre-exponential factor was calculated by compensation effect principle by ICTAC kinetics, whereas reaction mechanism was supposed by Master plots method.

Therefore, KAS had the following equation that uses the Murray-White approximation;

$$ln\left(\frac{\beta}{T^2}\right)=ln\left(\frac{A\cdot R}{E_\alpha\cdot g(\alpha)}\right)-\frac{E_\alpha}{R\cdot T} \qquad \text{KAS method} \tag{5}$$

Along with this, integration of Eq. (6) was done by taking the initial conditions i.e. $\alpha = 0$, at $T = T_0$. After that, introduction of Doyle's approximation followed by a few mathematical modifications [25] resulted in equation:

$$ln(\beta)=ln\left(\frac{A\cdot E_\alpha}{R\cdot g(\alpha)}\right)-\frac{E_\alpha}{R\cdot T} \qquad \text{FWO method} \tag{6}$$

Starink method uses the optimized by class of approximations minimizing the deviation between the approximation function and the exact integral.

$$ln\left(\frac{\beta}{T^{1.92}}\right)=\text{constant}-1.0008\cdot\frac{E_\alpha}{R\cdot T} \qquad \text{Starink Method} \tag{7}$$

kinetic parameters were calculated for a selected conversion point (α) by plotting (y-axis) the left side of each Eqs. (5)–(7) against the inverse of pyrolysis temperature (x-axis).

The previous isoconversional methods presented in Eqs. (6) and (7) can not predict the frequency factor and reaction model directly, thus, it is necessary the use of adequate methods for estimation of those parameters. The pre-exponential factor was estimated by linear relationship using the compensation effect, which requires using a model-fitting at a single heating rate. The ICTAC compensation effect uses different models (Table 1) to determine the compensation parameters (a and b) [26].

$$lnA=a\cdot E_\alpha+b \tag{8}$$

Several E_a and ln$A$ were obtained from Coats and Redfern (CR) model-fitting method which depends on asymptotic approximation $2RT/E_a \rightarrow 0$, giving following equation;

$$ln\left(\frac{g(\alpha)}{T^2}\right)=ln\left(\frac{A\cdot R}{E_\alpha\cdot\beta}\right)-\frac{E_\alpha}{R\cdot T} \qquad \text{CR Method} \tag{9}$$

For reaction model, the estimation was performed by master plot, which uses the overlap between the theoretical reference curves that are generated based on various reaction models for heterogeneous reactions (Table 1) and experimental findings of master plot obtained by the equality $g(\alpha)/g(0.5) = p(x)/p(x_{0.5})$ [27].

The kinetic parameters can be used to plot a simulated thermal profile solution from numerical method of Runge-Kutta 4th. The quality of fit (QOF), Correlation coefficient (R^2), and Root mean square error (RMSE) can be used to compare the experimental and simulated profiles.

$$RMSE=\sum\left(y_{exp}-y_{pre}\right)^2/N \tag{10}$$

Table 2
Proximate and Elemental Analysis of HT.

Proximate and Elemental Analysis								
VM (%)	Moisture (%)	Ash (%)	HHV (MJ kg^{-1})	C %	H %	O %	N %	S %
85–90	3–5	2.6–3.7	17–18	43–44	3–4	47–49	<3.5	<1

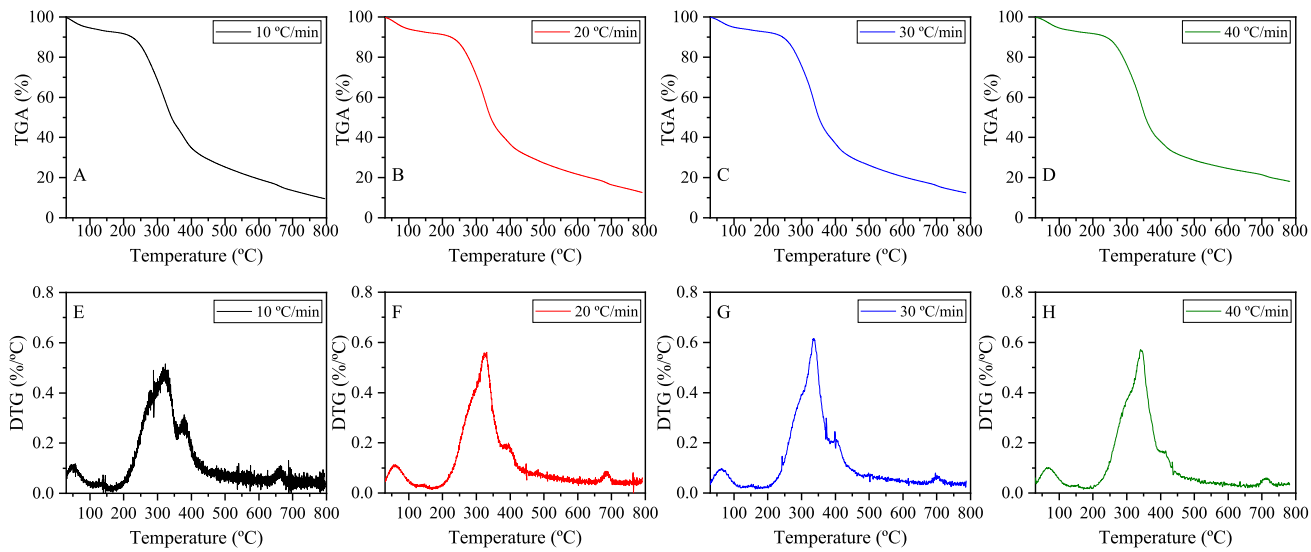

Fig. 1. (A-D) TG and (E-H) DTG curves of Holy Thistle (HT) at different heating rates.

$$QOF(\%) = 100 \cdot \left\{ 1 - \frac{\sqrt{RMSE}}{(y_{exp})_{max}} \right\} \tag{11}$$

$$R^2 = 1 - \frac{\sum (y_{exp} - y_{pre})^2}{\sum (y_{exp} - \bar{y}_{exp})^2} \tag{12}$$

where, y_{exp} is the experimental values measured, y_{pre} is the value calculated from the numerical method, $(y_{exp})_{max}$ is the high value measured experimentally, y_{exp} is the average of experimental values of dα/dt and N is the number of experimental data points used.

Results and discussion

Physicochemical parameters

HT biomass possessed elemental analysis results as shown in Table 2, where S is <1%. Due to the presence of lower nitrogen (<3.5%) and sulfur (<1%) content in the sample to conclude that the risk of emission of toxic gases i.e. NOx and SOx from pyrolysis is minimum. The range of volatile content (%) was observed within the range showed by the established bioenergy crops including Miscanthus gigantus and Arduno donax [28]. Moreover, proximate analysis was conducted to evaluate the feasibility of HT biomass for bioenergy application and thermochemical conversion process. The moisture contents (3–5 %), which is < 10% confirms its potential for pyrolysis [29]. Additionally, the high volatile matters content (85–90 %) and low ash content (2.6–3.7 %) supplements to the potential of HT biomass for substantial volatiles evolved during pyrolysis. While low carbon contents reflect its pyrolysis, enthalpy and capacity to deliver valued chemical instead of CO_2 release.

The amount of energy produced by the pyrolysis of biomass is indicated by the HHV. Predictive HHV of the sample was 17–18 MJ kg^{-1} that is considerably higher than the HHVs of many other famous energy crops including *Phalaris arundinacea* (*Reed canarygrass*), Para grass, A. donax (Giant reed), M. gigantus, , Salix spp. (Willow), and Camel grass, which had shown the HHVs as 17.2, 17.80, 16.30, 15.03, 15.10, and 15.00 MJ kg^{-1}, respectively [3,28,30–32].

Analyses of TG-DTG curves

TGA revealed the reaction chemistry and thermokinetics of the material at different heating rates and reaction temperature resulted to understand the major degradation patterns. During TGA analysis (TG-DTG curves), represented the thermochemical conversion of the biomass under different heating rates as shown in Fig. 1 (A and B). These curves showed specific trend, for the under studied samples, of the thermal degradation of lignocelluloses when they were put for the comparison to TG-DTG curves for Cardoon leaves, Red pepper waste, Camel grass, Elephant grass, Rice husk and Switchgrass [3,32–36].

During thermal degradation mass loss occur at certain temperature and these characteristic temperature are shown in Fig. 1 (A and B). Thermal conversion of the sample consists of three stages whereas stage-II had two zones. Temperature in the first stage reached up to 30–170 °C at all heating rates and resulted in the loss of 8 – 9 % of mass, which exhibits the extraction of the moisture fraction retained within intercellular spaces or compartments. In the second stage, all the heating rates were taken into account and temperature range was 170–450 °C that resulted in the maximum of the mass loss i.e. 55 – 60 %. There were two zones for all heating rates, and zone-I appeared between 170 and 380 °C whereas zone-II was present between 380 and 450 °C. In the third stage temperature was between 450 and 800 °C and this stage resulted about 15 % of the total mass lost.

Feasible biomass for pyrolysis contains <10% of the retained moisture, hence, the sample of the current study is a best choice for pyrolysis and combustion. Typical pattern of lignocellulose biomass was exhibited by thermal transformation. Here, stage-II was responsible for most of the thermal conversion, demonstrating the degradation of pectin, cellulose and hemicelluloses where a specific temperature of 170–450 °C was set for their degradation. Temperature ranges in the third stage reflected the degradation of lignin and formation of char [34]. Thermal transformation occurred up to 800 °C with average mass loss of 85 % – 88 %. Therefore, thermal conversion of HT biomass in different products could

Table 3
Temperature range for pyrolysis of each heating rate used experimentally.

Heating Rate (°C min^{-1})	Temperature (°C)	
	Initial	Final
10	116	469
20	116	507
30	116	521
40	116	537

Table 4
E_a and R^2 values at their respective conversion for the methods of FWO, KAS and Starink.

Conversion	FWO		KAS		Starink	
	E_α (kJ mol^{-1})	R^2	E_α (kJ mol^{-1})	R^2	E_α (kJ mol^{-1})	R^2
0.05	140.88	0.9231	139.80	0.9144	140.25	0.9148
0.1	143.44	0.9578	142.09	0.9527	142.55	0.9529
0.15	144.93	0.9336	143.41	0.9256	143.89	0.9259
0.2	142.32	0.9537	140.47	0.9477	140.95	0.9480
0.25	153.98	0.9625	152.59	0.9579	153.08	0.9581
0.3	156.80	0.9441	155.41	0.9374	155.91	0.9377
0.35	161.18	0.9439	159.88	0.9374	160.39	0.9376
0.4	165.32	0.9435	164.10	0.9369	164.62	0.9372
0.45	174.51	0.9267	173.64	0.9187	174.18	0.9191
0.5	190.03	0.9339	189.86	0.9272	190.41	0.9275
0.55	201.40	0.9160	201.70	0.9081	202.26	0.9084
0.6	211.90	0.8919	212.64	0.8825	213.21	0.8829
0.65	225.79	0.8609	227.12	0.8499	227.72	0.8503
0.7	250.54	0.8406	253.00	0.8294	253.62	0.8299
0.75	279.85	0.7461	283.61	0.7318	284.26	0.7324
0.8	249.31	0.7846	251.25	0.7698	251.89	0.7704
0.85	215.69	0.9220	215.66	0.9144	216.27	0.9147
0.9	169.10	0.9048	166.34	0.8927	166.94	0.8932
0.95	126.50	0.9295	120.99	0.9163	121.57	0.9169
Average	184.39	0.9063	183.87	0.8974	184.42	0.8978

be optimized in an energy efficient way by keeping the temperature in the above discussed range and lowering the heat rate. Keeping in view the above trend of these values, it is evident that using HT biomass for pyrolysis and combustion possesses significant advantage over previously studied biomass samples of water hyacinth, elephant grass, and rice husk [3,32,34,35,37]. Biochar yields of 24.59, 25.45 and 23.67% were determined at 387 °C at three different heating rates, and these yields were comparable to biochar obtained from the pyrolysis of bran (25.17%) and straw (23.68%) of rice plant, less than Camel (30.46%) [32], and Para grass (31.5%) [3]. These values suggest for the suitability of the sample for Biochar production.

Kinetics and thermodynamic parameters

The kinetic study of HT was performed using the thermogravimetric data in the decomposition region with a high mass loss rate (Table 3). Thus, the kinetic pyrolysis of HT was studied assuming a single-reaction model (single-step mechanism), i.e., the estimated kinetic data describes the behavior of the entire decomposition region present in Table 3.

The E_α of HT pyrolysis was calculated from the isoconversional methods of FWO, KAS and Starink for the conversion range of $0.05 \leq \alpha \leq 0.95$, where the results of E_a and coefficient of determination (R^2) are presented in Table 4

Table 4 shows a variation in the value of the R^2 values obtained by applying the isoconversional methods as a function of the conversion, where there is a conversion range with a value greater than 0.9 and other with conversion range < 0.9. The conversion range < 0.9 is in a small range between the conversion of 0.6–0.8, which is in the temperature region of 340–380 °C. In this temperature region, the thermogravimetric data presents different profiles of mass loss when comparing the curves for each heating rate. This behavior can be associated with different decomposition reactions that occur when the heating rate is increased, thus, resulting in a different profile, which reflects in the E_a values obtained when isoconversional methods are used. In general, the average values of E_a showed a coefficient of determination above 0.98. This value indicates that the methods used to obtain the E_a values can describe the pyrolysis reaction for chosen

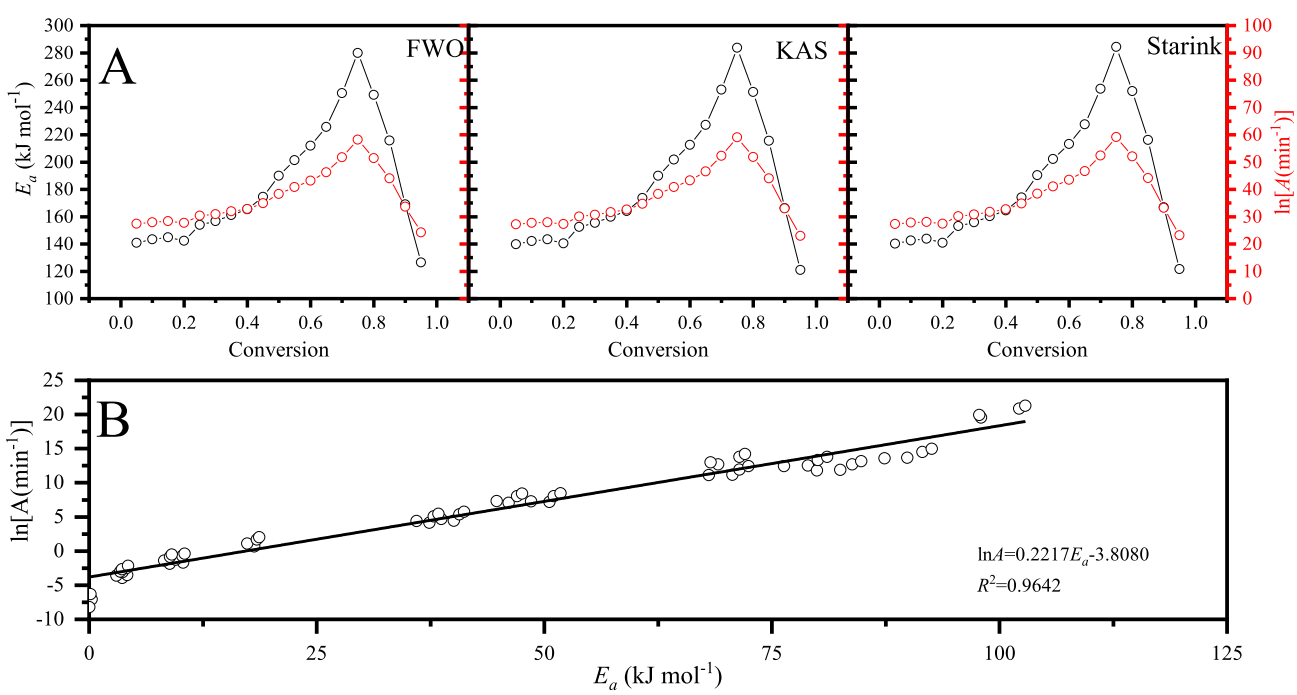

Fig. 2. (A) Profiles of Ea versus conversion and lnA versus conversion for each isoconversional method and (B) linear adjustment obtained through the compensation effect.

Table 5
Pre-exponential factor found based on compensation effect and using the E_a value from FWO, KAS and Starink.

Conversion	Pre-exponential factor (min^{-1})		
	FWO	KAS	Starink
0.05	8.09×10^{11}	6.37×10^{11}	7.03×10^{11}
0.1	1.43×10^{12}	1.06×10^{12}	1.17×10^{12}
0.15	1.99×10^{12}	1.42×10^{12}	1.58×10^{12}
0.2	1.11×10^{12}	7.38×10^{11}	8.21×10^{11}
0.25	1.47×10^{13}	1.08×10^{13}	1.21×10^{13}
0.3	2.76×10^{13}	2.03×10^{13}	2.26×10^{13}
0.35	7.27×10^{13}	5.45×10^{13}	6.11×10^{13}
0.4	1.82×10^{14}	1.39×10^{14}	1.56×10^{14}
0.45	1.40×10^{15}	1.15×10^{15}	1.30×10^{15}
0.5	4.36×10^{16}	4.19×10^{16}	4.73×10^{16}
0.55	5.41×10^{17}	5.78×10^{17}	6.55×10^{17}
0.6	5.55×10^{18}	6.53×10^{18}	7.43×10^{18}
0.65	1.21×10^{20}	1.62×10^{20}	1.85×10^{20}
0.7	2.91×10^{22}	5.01×10^{22}	5.76×10^{22}
0.75	1.93×10^{25}	4.44×10^{25}	5.13×10^{25}
0.8	2.21×10^{22}	3.41×10^{22}	3.93×10^{22}
0.85	1.29×10^{19}	1.28×10^{19}	1.46×10^{19}
0.9	4.21×10^{14}	2.29×10^{14}	2.61×10^{14}
0.95	3.34×10^{10}	9.85×10^{9}	1.12×10^{10}
Average	1.25×10^{16}	1.11×10^{16}	1.26×10^{16}

temperature range.

Table 4 shows a significant increase in the value of E_a between the start of pyrolysis ($\alpha = 0.05$) until a conversion of 0.75 (maximum value of E_a). This behavior indicates that the solid structure remaining in each conversion has its intermolecular forces increased (C–C bonds), therefore, that keep them in their solid state. Thus, a greater amount of energy (heat) is required for these interactions to be undone and light molecular structures released (volatile). This behavior occurs for conversion range that comprises the high mass loss rates observed in the thermogravimetric curves. The increase in the value of E_a was 140.88–279.85 kJ mol^{-1}, 139.80–283.61 kJ mol^{-1} and 140.25–284.26 kJ mol^{-1}, for KAS, FWO and Starink, respectively. In this conversion range, the HT decomposes by parallel reactions, which makes it difficult to estimate each value. On the other hand, most of the hemicelluloses and some compounds with less thermal stability were eliminated, thus in the conversion of 0.75 can be related to cellulose. Similar E_a values were observed by Chen et al. [38] in the pyrolysis of the biomass components, which obtained values between 227.27 and 287.56 kJ mol^{-1} for cellulose and < 200 kJ mol^{-1} for hemicelluloses. A decrease in the value of E_a is observed in the conversion range between 0.75 and 0.95, which indicates a lower thermal stability. This behavior is related in the cleavage reaction of C-O, C–C and β-O-4 bonds present in lignin and which present values of $E_a < 100$ kJ mol^{-1} and decomposes in the whole experimental temperature range [38,39].

The evaluation of pyrolysis kinetics through a single-step has the advantage to generate a small amount of data with satisfactory information when the thermal decomposition is represented by a single peak, as obtained from wood pyrolysis. In addition, these parameters are suitable for simulation of thermal process in real reactors, since these simplified data facilitate the processing speed by the smaller number of parameters by those obtained from parallel reactions evaluation. The satisfactory applicability of the kinetic parameters considering their average values is observed in the study on the simulation of spherical wood particles in a fluidized bed reactor carried out by di Celso et. al. Thus, the average E_a values obtained for the isoconversional methods of KAS, FWO and Starink were 184.39 kJ mol^{-1}, 183.87 kJ mol^{-1} and 184.42 kJ mol^{-1}, respectively. The average value of E_a were similar to those observed for Azadirachta indica seeds (176.66–196.06 kJ mol^{-1}), Phyllanthus emblica seeds (184.77–195.10 kJ mol^{-1}), Samanea saman seeds (187.20–204.93 kJ mol^{-1}) and Rice food waste (203.20–220.29 kJ mol^{-1}) [40–42].

The values of A and f(α) were estimated by compensation effect and master plot, since the isoconversional methods are unable to extract those parameters. The activation energy values from most accurate isoconversional method were used together with the compensation effect and master plot for obtaining these kinetic parameters.

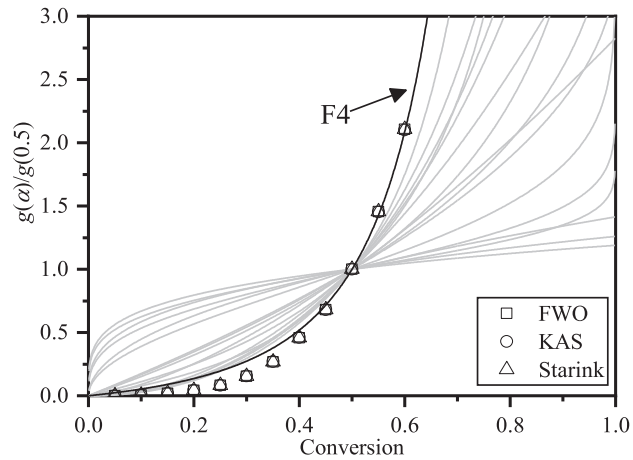

Fig. 3. Overlapping between experimental and theoretical curves of g(α)/g (0.5) for HT pyrolysis.

Fig. 2 shows a satisfactory value of R^2, which was above 0.9. This R^2 value indicates that the pre-exponential can be estimated by the compensation parameters obtained from linear adjustment. The compensation parameters obtained for the pyrolysis of HT were 0.2217 and −3.8080 for a and b, respectively. Thus, applying the E_a values and the compensation parameters are obtained the A values showed in Table 5.

The A values change in a high range due the linear relationship of compensation effect that promotes similar behavior to E_a values and indicates the complexity of the pyrolysis reaction of *HT*. The pre-exponential factor indicates collision rate in a reaction, where this value is directly associated with the energy requirement for product generation. High values of A ($>6 \times 10^9$ min^{-1}) indicate higher molecular collision that requires more heat to be transferred [43]. Frequency factor based in the average value of E_α for methods of FWO, KAS and Starink were 1.25×10^{16} min^{-1}, 1.11×10^{16} min^{-1} and 1.26×10^{16} min^{-1}, respectively.

Fig. 3 showed the master plot based on the overlap between the experimental data calculated from integral form of the kinetic data (p (x)/($x_{0.5}$) vs conversion) and theoretical curve (g(α)/g(0.5) vs conversion). The overlap between these curves helps to proper indicate the reaction model that deliver the optimal fitting of the experimental data. The reaction model for HT pyrolysis is described by an n-order reaction model as observed in Fig. 3. The fourth-order reaction model (F4) may demonstrates the decomposition process by single-step mechanism, even though several reactions may take place simultaneously. The n-order model is the simplest and most suitable model for use in real process simulation, being similar to the one used in homogeneous kinetics. In these models, the reaction rate is proportional to the concentration of the residual reagent concentration to a certain potency [44]. Wang et al. [3] evaluated the pyrolysis of lignocellulosic components (hemicellulose, hemicellulose, and lignin) present in the biomass. This study showed that lignin pyrolysis has a high reaction order ($n = 12$), which is due to the complexity of the chemical structure and different thermal stabilities as it is decomposed. Compared to hemicellulose and cellulose, which presented order of reaction in the order of $n = 1$–3, lignin may limit the potency of the global reaction kinetics, which justifies the F4 order of reaction obtained in the current study.

Order-based in those models are the simplest as they are similar to those used in homogeneous kinetics. In these models, the reaction rate is proportional to concentration, amount or fraction remaining of reactant

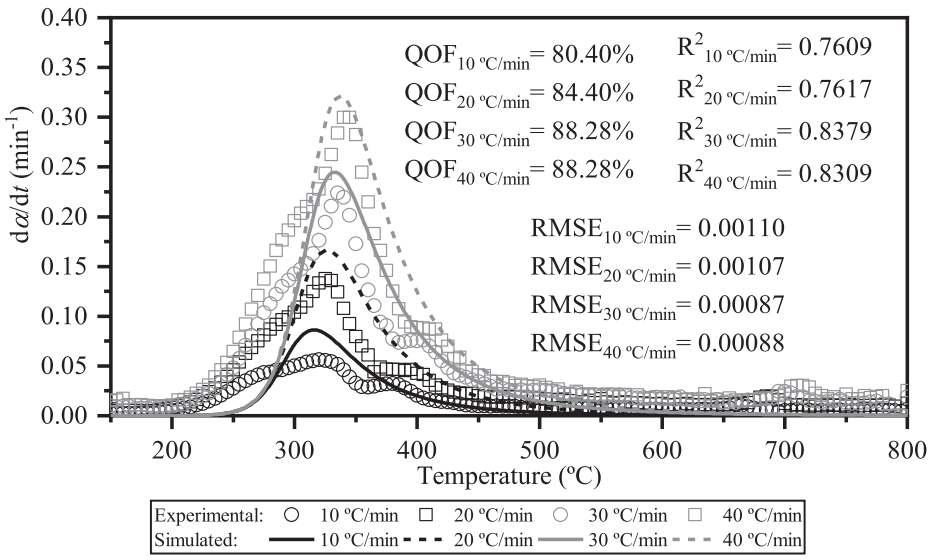

Fig. 4. Experimental vs Simulated Results of Holy Thistle Pyrolysis process.

(s) raised to a particular power (integral or fractional) which is the reaction order.

The kinetic triplet (E_a, A, and f(α)) represents the pyrolysis process mathematically, thus, these parameters can be used to plot the curves of thermal behavior. Thus, the Eq. (13) can describe mathematically the pyrolysis of HT, and the reconstructed curves of the dα/dt versus T (Fig. 4) can be obtained by numerical method of Runge-Kutta 4th.

$$\frac{d\alpha}{dt} = 1.11 \cdot 10^{16} \cdot exp\left(\frac{-183870}{R \cdot T}\right) \cdot (1-\alpha)^4 \quad (13)$$

The overlapping of the experimental and simulated data resulted in a behavior that satisfactorily describes the pyrolysis process. This satisfactory adjustment can be observed by the QOF values that was greater than 80% (R^2 greater than 0.76) for the simulated curves in the HT pyrolysis. This value indicates that the data has a low deviation between the experimental and simulated values, although the kinetic parameter estimation by the single-step mechanism. A smaller adjustment is observed in the decomposition region where a "shoulder" occurred (temperatures of 227–287 °C), which is associated with the assumption of the reaction occurring in a global process (single-step mechanism) and disregard of parallel reactions. On the other hand, the use of the global process for HT was favored by its thermal behavior, since it presents only one thermal decomposition peak, which results in an approximately similar behavior as observed in Fig. 4. Thus, the use of kinetic parameters in relation to its average values satisfactorily satisfies the thermal behavior. the kinetic parameters obtained can represent a simple alternative for the application in the simulation of pyrolytic reactors due to their satisfactory approximation of the experimental data. Such applications are noted in the works by Ding et al. and Di Celso et al., which use mathematical tools, such as kinetic data, to predict the thermal behavior of reactions such as wood combustion and pyrolysis in a fluidized bed reactor before the gasifier [45,46].

Conclusion

The best suitable temperature for HT was 170 – 450 °C at which major pyrolysis products could be obtained. The average E_α values obtained by FWO, KAS, and Starink were between 183 and 185 kJ mol^{-1}. The higher HHV value (17.24 MJ kg^{-1}) was observed against many other established energy crops. Experimental data was compared to the simulation driven predicted data points and resulted in best-fit plots. Last but not the least, from the reaction mechanism for pyrolysis experiment had fourth-order reaction model (F4) that may demonstrates the decomposition process by single-step mechanism, even though several reactions may take place simultaneously. The current research was focused to explore best reaction conditions of pyrolysis process for HT to obtain products and chemicals as an alternative to traditional energy resources. The study revealed that Holy thistle would be a promising feedstock for bioenergy generation through pyrolysis and co-pyrolysis process. The current research was critical to explore the kinetic and thermodynamic parameters of HT to build biorefinery and bioenergy reactors design in future perspectives.

Declaration of Competing Interest

The authors declare that they have no known competing financial interests or personal relationships that could have appeared to influence the work reported in this paper.

Acknowledgments

This project was funded by the Deanship of Scientific Research (DSR) at King Abdulaziz University, Jeddah under grant no. (RG-5-135-41). The authors, therefore, acknowledge with thanks DSR technical and financial support.

References

[1] Pfeiffer DA. Eating fossil fuels: oil, food, and the coming crisis in agriculture. New Society Publishers; 2006.
[2] Zhang B, Yang J, Cao Y. Assessing Potential Bioenergy Production on Urban Marginal Land in 20 Major Cities of China by the Use of Multi-View High-Resolution Remote Sensing Data. Sustainability 2021;13(13):7291. https://doi.org/10.3390/su13137291.
[3] Ahmad MS, Mehmood MA, Al Ayed OS, Ye G, Luo H, Ibrahim M, et al. Kinetic analyses and pyrolytic behavior of Para grass (Urochloa mutica) for its bioenergy potential. Bioresour Technol 2017;224:708–13.
[4] Mettler MS, Vlachos DG, Dauenhauer PJ. Top ten fundamental challenges of biomass pyrolysis for biofuels. Energy & Environ Sci 2012;5:7797–809.
[5] Alhumade H, da Silva JCG, Ahmad MS, Çakman G, Yıldız A, Ceylan S, et al. Investigation of pyrolysis kinetics and thermal behavior of Invasive Reed Canary (Phalaris arundinacea) for bioenergy potential. J Anal Appl Pyrol 2019;140:385–92. https://doi.org/10.1016/j.jaap.2019.04.018.
[6] Konur O. Biomass pyrolysis and pyrolysis oils: A review of the research. Biodiesel Fuels 2021:153–69.
[7] Zhou S, Xue Y, Cai J, Cui C, Ni Z, Zhou Z. An understanding for improved biomass pyrolysis: Toward a systematic comparison of different acid pretreatments. Chem Eng J 2021;411:128513.
[8] Xu M, Zhu X, Li X, Hu Z, Huang Y, Xia Ao, et al. Investigation of the combustion behaviors and kinetic modelling of municipal solid waste char under isothermal

conditions using a micro-fluidized bed. J Environ Chem Eng 2021;9(5):105984. https://doi.org/10.1016/j.jece:2021.105984.
[9] Rezende ML, Richardson JW. Risk analysis of using sweet sorghum for ethanol production in southeastern Brazil. Biomass Bioenergy 2017;97:100–7. https://doi.org/10.1016/j.biombioe.2016.12.016.
[10] Paniagua S, Prado-Guerra A, García AI, Calvo LF. Bioenergy derived from an organically fertilized poplar plot: overall TGA and index estimation study for combustion, gasification, and pyrolysis processes. Biomass Convers Biorefinery 2019;9(4):749–60. https://doi.org/10.1007/s13399-019-00392-7.
[11] Nguyen TTH, Nguyen XC, Nguyen DLT, Nguyen DD, Vo TYB, Vo QN, Nguyen TD, Ly QV, Ngo HH, Vo D-VN. et al. Converting biomass of agrowastes and invasive plant into alternative materials for water remediation. Biomass Convers. Biorefinery 2021, 1–16.
[12] Jarolin K, Wang S, Dymala T, Song T, Heinrich S, Shen L, et al. Characterizing devolatilized wood pellets for fluidized bed applications. Biomass Convers Biorefinery 2021:1–18.
[13] Mu L, Wang R, Zhai Z, Zhang B, Shang Y, Yin H. Evaluation of thermokinetics methodology, parameters, and coke characterization of co-pyrolysis of bituminous coal with herbaceous and agricultural biomass. Biomass Convers Biorefinery 2021:1–16.
[14] Amaku JF, Nnaji JC, Ogundare SA, Akpomie KG, Ngwu CM, Chukwuemeka-Okorie HO, et al. Chrysophyllum albidum stem bark extract coated tillite adsorbent for the uptake of Cr (VI): thermodynamic, kinetic, isotherm, and reusability. Biomass Convers Biorefinery 2021:1–13.
[15] Saldarriaga JF, Montoya NA, Estiati I, Aguayo AT, Aguado R, Olazar M. Unburned material from biomass combustion as low-cost adsorbent for amoxicillin removal from wastewater. J Clean Prod 2021;284:124732.
[16] Zhai J, Burke IT, Mayes WM, Stewart DI. New insights into biomass combustion ash categorisation: A phylogenetic analysis. Fuel 2021;287:119469. https://doi.org/10.1016/j.fuel.2020.119469.
[17] He C-R, Kuo Y-Y, Li S-Y. Lignocellulosic butanol production from Napier grass using semi-simultaneous saccharification fermentation. Bioresour Technol. 2017;231:101–8.
[18] Ussiri DAN, Lal R. The Role of Bioenergy in Mitigating Climate Change. In: Ussiri DAN, Lal R, editors. Carbon Sequestration for Climate Change Mitigation and Adaptation. Cham: Springer International Publishing; 2017. p. 433–95. https://doi.org/10.1007/978-3-319-53845-7_12.
[19] Trninić M, Wang L, Várhegyi G, Grønli M, Skreiberg Ø. Kinetics of corncob pyrolysis. Energy Fuels 2012;26:2005–13.
[20] Nhuchhen DR, Salam PA. Estimation of higher heating value of biomass from proximate analysis: A new approach. Fuel 2012;99:55–63.
[21] Vyazovkin S, Burnham AK, Criado JM, Pérez-Maqueda LA, Popescu C, Sbirrazzuoli N. ICTAC Kinetics Committee recommendations for performing kinetic computations on thermal analysis data. Thermochim. Acta 2011;520:1–19.
[22] Akahira T, Sunose T. Transactions of Joint Convention of Four Electrical Institutes. 1969, 246.
[23] Flynn JH, Wall LA. A quick, direct method for the determination of activation energy from thermogravimetric data. J. Polym Sci Part B Polym Lett 1966;4:323–8.
[24] Ozawa T. A new method of analyzing thermogravimetric data. Bull Chem Soc Jpn. 1965;38:1881–6.
[25] Doyle CD. Kinetic analysis of thermogravimetric data. J Appl Polym Sci 1961;5:285–92.
[26] Vyazovkin S, Chrissafis K, Di Lorenzo ML, Koga N, Pijolat M, Roduit B, et al. ICTAC Kinetics Committee recommendations for collecting experimental thermal analysis data for kinetic computations. Thermochim Acta 2014;590:1–23. https://doi.org/10.1016/j.tca.2014.05.036.
[27] Gotor FJ, Criado JM, Malek J, Koga N. Kinetic Analysis of Solid-State Reactions: The Universality of Master Plots for Analyzing Isothermal and Nonisothermal Experiments. J Phys Chem A 2000;104:10777–82. https://doi.org/10.1021/jp0022205.
[28] Jeguirim M, Dorge S, Trouvé G. Thermogravimetric analysis and emission characteristics of two energy crops in air atmosphere: Arundo donax and Miscanthus giganthus. Bioresour Technol 2010;101:788–93.
[29] Tahir MH, Çakman G, Goldfarb JL, Topcu Y, Naqvi SR, Ceylan S. Demonstrating the Suitability of Canola Residue Biomass to Biofuel Conversion via Pyrolysis through Reaction Kinetics, Thermodynamics and Evolved Gas Analyses. Bioresour. Technol. 2019.
[30] Howaniec N, Smoliński A. Steam gasification of energy crops of high cultivation potential in Poland to hydrogen-rich gas. Int J Hydrogen Energy 2011;36(3):2038–43.
[31] Paulrud S, Nilsson C. Briquetting and combustion of spring-harvested reed canary-grass: effect of fuel composition. Biomass Bioenergy 2001;20(1):25–35.
[32] Mehmood MA, Ye G, Luo H, Liu C, Malik S, Afzal I, et al. Pyrolysis and kinetic analyses of Camel grass (Cymbopogon schoenanthus) for bioenergy. Bioresour. Technol. 2017;228:18–24.
[33] Xu Y, Chen B. Investigation of thermodynamic parameters in the pyrolysis conversion of biomass and manure to biochars using thermogravimetric analysis. Bioresour. Technol. 2013;146:485–93.
[34] Braga RM, Melo DMA, Aquino FM, Freitas JCO, Melo MAF, Barros JMF, et al. Characterization and comparative study of pyrolysis kinetics of the rice husk and the elephant grass. J Therm AnalCalorim. 2014;115:1915–20.
[35] Biney PO, Gyamerah M, Shen J, Menezes B. Kinetics of the pyrolysis of arundo, sawdust, corn stover and switch grass biomass by thermogravimetric analysis using a multi-stage model. Bioresour Technol 2015;179:113–22.
[36] Maia AAD, de Morais LC. Kinetic parameters of red pepper waste as biomass to solid biofuel. Bioresour Technol 2016;204:157–63.
[37] Huang L, Liu J, He Y, Sun S, Chen J, Sun J, et al. Thermodynamics and kinetics parameters of co-combustion between sewage sludge and water hyacinth in CO 2/O 2 atmosphere as biomass to solid biofuel. Bioresour Technol 2016;218:631–42.
[38] Chen W-H, Eng CF, Lin Y-Y, Bach Q-V. Independent parallel pyrolysis kinetics of cellulose, hemicelluloses and lignin at various heating rates analyzed by evolutionary computation. Energy Convers Manag 2020;221:113165.
[39] Collard F-X, Blin J. A review on pyrolysis of biomass constituents: Mechanisms and composition of the products obtained from the conversion of cellulose, hemicelluloses and lignin. Renew Sustain Energy Rev 2014;38:594–608.
[40] Mishra RK, Sahoo A, Mohanty K. Pyrolysis kinetics and synergistic effect in co-pyrolysis of Samanea saman seeds and polyethylene terephthalate using thermogravimetric analyser. Bioresour Technol 2019;289:121608.
[41] Ming X, Xu F, Jiang Y, Zong P, Wang B, Li J, et al. Thermal degradation of food waste by TG-FTIR and Py-GC/MS: Pyrolysis behaviors, products, kinetic and thermodynamic analysis. J Clean Prod 2020;244:118713.
[42] Mishra RK, Mohanty K. Kinetic analysis and pyrolysis behaviour of waste biomass towards its bioenergy potential. Bioresour Technol 2020;311:123480.
[43] Ahmad MS, Klemeš J, Alhumade H, Elkamel A, Mahmood A, Shen B, et al. Thermo-kinetic study to elucidate the bioenergy potential of Maple Leaf Waste (MLW) by pyrolysis, TGA and kinetic modelling. Fuel 2021;293:120349. https://doi.org/10.1016/j.fuel.2021.120349.
[44] Khawam A. D.R.F. Solid-state kinetic models: basics and mathematical fundamentals. J Phys Chem B 2006;110:17315–28.
[45] di Celso GM, Rapagnà S, Prisciandaro M, Zanoelo EF. Kinetics of pyrolysis and combustion of spherical wood particles in a fluidized bed. Energy Convers Manag 2014;82:27–36.
[46] Ding Y, Ezekoye OA, Zhang J, Wang C, Lu S. The effect of chemical reaction kinetic parameters on the bench-scale pyrolysis of lignocellulosic biomass. Fuel 2018;232:147–53.